Synchrotron X-ray Absorption and *In Vitro* Bioactivity of Magnetic Macro/Mesoporous Bioactive Glasses

Regular Paper

Thanida Charoensuk[1], Wanwisa Limphirat[2], Chitnarong Sirisathitkul[1]*, Witoon Tangwatanakul[3], Pongsakorn Jantaratana[4] and Upsorn Boonyang[1]

1 Molecular Technology Research Unit, School of Science, Walailak University, Nakhon Si Thammarat, Thailand
2 Synchrotron Light Research Institute, Nakhon Ratchasima, Thailand
3 Faculty of Science and Technology, Nakhon Si Thammarat Rajabhat University, Nakhon Si Thammarat, Thailand
4 Department of Physics, Faculty of Science, Kasetsart University, Bangkok, Thailand
*Corresponding author(s) E-mail: chitnarong.siri@gmail.com

Abstract

Iron oxides in macro/mesoporous bioactive glasses were characterized by synchrotron X-ray absorption near edge structure (XANES) spectroscopy. This magnetic phase was introduced by adding $Fe(NO_3)_3 \cdot 9H_2O$ during the sol-gel synthesis. The obtained bioactive glass scaffolds exhibited superparamagnetism, in which the magnetization was increased with the increase in the Fe molar ratio from 10 to 20%. The linear combination fits of the XANES spectra indicated that the increase in the Fe molar ratio to 20% enhanced the γ-Fe_2O_3 formation at the expense of the α-Fe_2O_3 phase. This variation also promoted the formation of fine-grained bone-like apatites on the surface of the scaffolds in the *in vitro* test. The apatite growth between three and seven days was confirmed by the changing elemental compositions. However, the highest magnetic proportion led to the distortion of the skeleton walls and the collapse of the porous networks.

Keywords Macro/mesoporous Bioactive Glass, Sol-gel Method, Superparamagnetism, XANES, *In vitro* Test

1. Introduction

Porous bioactive glass scaffolds have been under research and development for the regeneration of bone defects [1, 2]. Their bioactivity and biodegradability are vastly enhanced compared with traditional bioactive glasses, due to large surface areas in the mesostructures [3, 4]. Moreover, *in vitro* tests on bioactive glasses combined with other phases have been reported [5, 6]. By incorporating magnetic nanoparticles, the obtained bioactive glasses can be implemented in local hyperthermia treatments. In response to alternating magnetic fields, heat is generated to eliminate cancerous tissues around the bone defects [7–9]. Local drug delivery can also be added to prevent the transportation of cancer cells to other sites [9–11]. To realize the commercial potential of these multifunctional bioactive glasses, attempts have been made to determine the influence of process parameters on the distribution of pores, magnetic properties and bioactivity.

Magnetic bioactive glasses have mostly been obtained from the sol-gel synthesis [10, 12–14]. The sizes of the macro-pores are commonly between 200 and 500 μm, whereas the

Sample Code	Composition of SiO₂-CaO-Na₂O-P₂O₅-Fe₂O₃ (%mol)	P123 (g)	TEOS (ml)	TEP (ml)	NaNO₃ (ml)	Ca(NO₃)₂· 4H₂O (g)	Fe(NO₃)₃· 9H₂O (g)	(1M)HNO₃ (ml)	EtOH (ml)
65S10Fe	65-15-5-5-10	0.542	1.46	0.15	1.00	0.354	0.404	1.00	2.50
65S15Fe	65-10-5-5-15	0.543	1.46	0.15	1.00	0.237	0.607	1.00	2.50
65S20Fe	65-5-5-5-20	0.542	1.46	0.15	1.00	0.118	0.808	1.00	2.50
60S20Fe	60-10-5-5-20	0.506	1.34	0.15	1.00	0.236	0.809	1.00	2.50

Table 1. Composition of reagents used in the sol-gel synthesis of magnetic bioactive glass scaffolds

average diameter of the mesopores is in the range of 3-5 nm [8, 9, 13]. Interestingly, X. Li et al. reported a reduction in pore size of CaO-P₂O₅-SiO₂/Fe₃O₄ glass with an increase in Ca concentrations and a decrease in Fe concentrations [11]. From the point of view of application, the biocompatibility of macro/mesoporous bioactive glasses with a magnetic phase was tested and confirmed [8–10, 12, 13]. The growth of apatites in the *in vitro* test is one of the common indicators of bioactivity. However, it is observed that the apatite-forming ability and cell attachment tend to decrease with an increase in the magnetic phase in bioactive glasses [15]. In addition to bioactivity tests, the capability of the drug loading-release was also demonstrated [9, 11, 13].

Superparamagnetic properties of bioactive glass scaffolds are reportedly attributed to different forms of iron oxides added during the synthesis or formed in the calcination step. For example, magnetite (Fe₃O₄) nanoparticles are distributed in the walls between mesopores in the works of Wang et al. [8] and Li et al. [11], whereas a maghemite (γ-Fe₂O₃) phase was detected by M. Zhu et al. [13]. In addition to these iron oxides, manganese ferrite [12] and zinc ferrite [16] were successfully introduced as a soft magnetic phase with a narrow hysteresis loop and low coercivity in a bioactive glass matrix. Furthermore, a mixed phase with more than one type of magnetic nanoparticles may be obtained [17].

In this work, bioactive glass scaffolds are magnetically tuned by varying the molar ratios of iron in the synthesis and the effect of the magnetic phase on bioactivity is investigated. In addition to elemental composition and magnetic measurements, synchrotron X-ray absorption near edge structure (XANES) spectra are analysed to study the mixed iron oxide phase, which contributes to the desirable bioactivity and magnetic properties for implementations.

2. Materials and Methods

Magnetic bioactive glass scaffolds were synthesized by using the one-pot sol-gel method. Four samples, i.e., 65S10Fe, 65S15Fe, 65S20Fe and 60S20Fe, were obtained from varying compositions of starting reagents listed in Table 1. Poly-methyl methacrylate (PMMA) colloidal crystals were used as the three-dimensionally ordered macroporous (3DOM) structure template. Poly(ethylene glycol)-block-poly(propylene glycol)-block-poly(ethylene

glycol) (P123) acted as both the mesoporous structure-directing agent and the reducing agent for Fe. Solutions of P123, Ca(NO₃)₂ 4H₂O and Fe(NO₃)₃ 9H₂O in ethanol were gradually added drop-by-drop and mixed with tetraethyl orthosilicate (TEOS), triethyl phosphate (TEP) and NaNO₃. The solution was vigorously stirred (∼700 rpm) at room temperature and HNO₃ was added as the catalyst. The stirring was terminated when the solution reached the gel point and the PMMA colloidal crystals were soaked in the solution. The excess solution was removed after the complete immersion. The samples were aged in the sealed vials at 45° C for one day, allowing a continuous polycondensation reaction. They were then dried at 45° C for one day to eliminate excess solutions. Finally, the dried samples were calcined at 600° C for 6 h with a heating rate of 2° C/min and a cooling rate of 20° C/min.

The calcined samples were characterized for their physical properties and bioactivity. The field emission scanning electron microscope (FESEM: Zeiss Supra 55VP), operated at 20 kV, gave details of the structure, size and shape of the skeleton walls and the windows between the macropores. Each sample was coated with a conductive carbon layer to prevent charge accumulation. The energy dispersive spectrometry (EDS: Zeiss Evo LS15 with a Bruker EDS Quantax 400) with the detectors attached to the FESEM was used to determine the elemental compositions of the scaffolds. To identify the structure of the magnetic phase, the XANES spectra were measured at BL-8 Synchrotron Light Research Institute, Thailand. Samples were prepared by grinding dried powder in a mortar to reduce the grain size. They were then thinly dispersed on the substrate and covered by polyimide tape. The Fe K-edge spectra were collected at room temperature in the fluorescent mode with ionization chambers and 13-array Ge detectors placed before and on the left-hand side of the sample. In the measurement, the photon energy was scanned from -100 eV below the edge to 300 eV above the edge by a Ge(220) double crystal monochromator. For the linear combination fitting (LCF), Fe, FeO, Fe₃O₄, γ-Fe₂O₃, and α-Fe₂O₃ standards were also measured as references. The XANES spectra were normalized after pre-edge and post-edge subtractions and fitted using the Athena program [18].

To examine the magnetic properties at room temperature, the magnetizations of the bioactive glass scaffolds in response to the varying magnetic fields between -10 kOe and 10 kOe were measured by means of vibrating sample
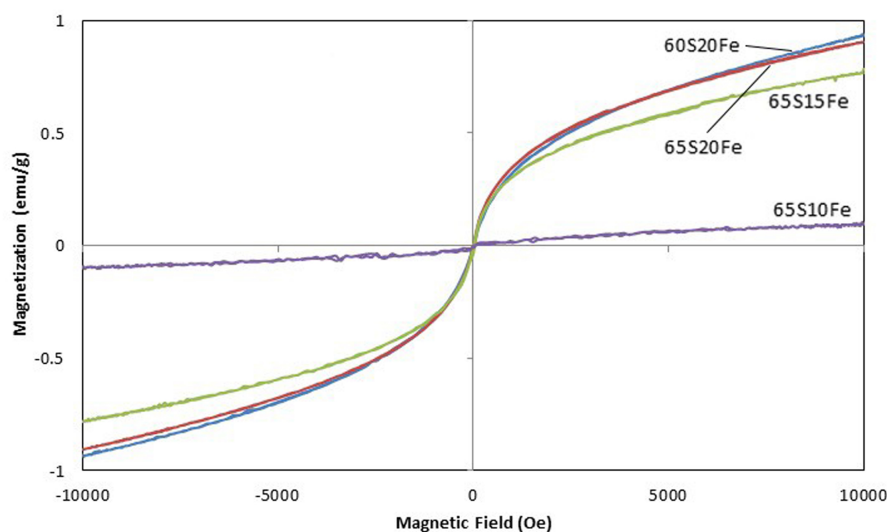
Figure 1. Magnetization curves showing superparamagnetic behaviours of samples 65S10Fe, 65S15Fe, 65S20Fe and 60S20Fe

magnetometry (VSM). In the *in vitro* bioactivity test at body temperature (37° C) using the Kokubo method [19], the samples 65S15Fe and 60S20Fe were immersed in the stimulated body fluid (SBF), whose composition and ionic concentration similar to human blood plasma was detailed in the previous report [20]. The formation of the apatite phase was monitored by FESEM after a half, one, three and five days. For the samples after three and seven days, X-ray diffractometry (XRD) was carried out by Philips X'Pert using Cu Kα radiation in the 2θ range of 10-50 degrees with 2 degrees/min for each step.

3. Results and Discussion

The variation in magnetization of each bioactive glass scaffold in response to an applied magnetic field, as shown in Figure 1, confirms that the magnetic phase is successfully introduced. The magnetization, induced in the direction of the increasing magnetic field up to 10 kOe, is enhanced by the increase in Fe(NO$_3$)$_3$ 9H$_2$O from 10 to 20% mol in the synthesis. While samples 65S20Fe and 60S20Fe have much higher magnetizations than that of sample 65S10Fe, all the bioactive glass scaffolds similarly exhibit a linear increase of magnetizations in the low field regime. The slope of changing magnetization is gradually reduced beyond 5 kOe, but saturation is not obtained under the maximum magnetic field of 10 kOe. When the applied magnetic field is decreased back to 0 kOe, each magnetization curve is virtually traced back to the same path. The minimal hysteresis and coercive field are characteristics of superparamagnetism. In these bioactive glass scaffolds, the superparamagnetic behaviour is attributed to iron oxide nanoparticles whose sizes are in the single-domain regime.

From structural analysis of iron oxides by XANES, the overall characteristics of XANES spectra in Figure 2, including the pre-edge, are similar for all four bioactive glass scaffolds. Each spectrum is compared with four standards, namely FeO, Fe$_3$O$_4$, α-Fe$_2$O$_3$ and γ-Fe$_2$O$_3$. Since

the spectra of bioactive glass scaffolds are not identical to any single standard, the iron oxides are decidedly in the mixed phase. The pre-edge match further suggests a majority of Fe^{3+}. The corundum-structured α-Fe$_2$O$_3$ and spinel-structured γ-Fe$_2$O$_3$ are therefore used in the LCF fitting and the simulated spectra are plotted in dotted lines for comparison. The fitting is very good up to 7125 eV, whereas the discrepancy at higher energy is likely to be due to the presence of Fe$_3$O$_4$ and the self-absorption in fluorescence spectra. While α-Fe$_2$O$_3$ is the dominant phase in samples 65S10Fe and 65S15Fe, the XANES fits indicate that samples 65S20Fe and 60S20Fe have a higher proportion of γ-Fe$_2$O$_3$. Such preference of γ-Fe$_2$O$_3$ over α-Fe$_2$O$_3$ enhances the magnetization in these samples, as previously shown in Figure 1. The reduction in the intensity and width of the absorption peak in Figures 2(c) and 2(d) can also be explained by the increase in the γ-Fe$_2$O$_3$ proportion.

According to an FESEM image in Figure 3(a), the 3DOM structure is inherited from the PMMA template during the sol-gel synthesis and the network of hexagonal pores is extended over the piece of scaffold. However, the skeletal walls are increasingly distorted by the rise of the magnetic phase in Figures 3(b)-3(d). In addition to the wall distortion, a high molar ratio of Fe apparently disrupts the arrangement of the template during the synthesis and leads to the subsequent collapse of the porous network. After soaking in SBF solutions for half a day, the bone-like apatite starts to form on the walls in sample 65S15Fe. By tracking surface changes for up to five days (Figure 4), it can be seen that the bone-like apatite phase increases with the increased soaking time until the porous surfaces are fully covered. The bioactivity is increased by the rise in the magnetic phase as the bone-like apatite is formed with a smaller grain and a higher rate (Figure 5). The surface of sample 60S20Fe is densely packed with fine grains after only one day. This increased bioactivity is linked to the biocompatibility of the γ-Fe$_2$O$_3$ phase present in this sample [21–23]. While the
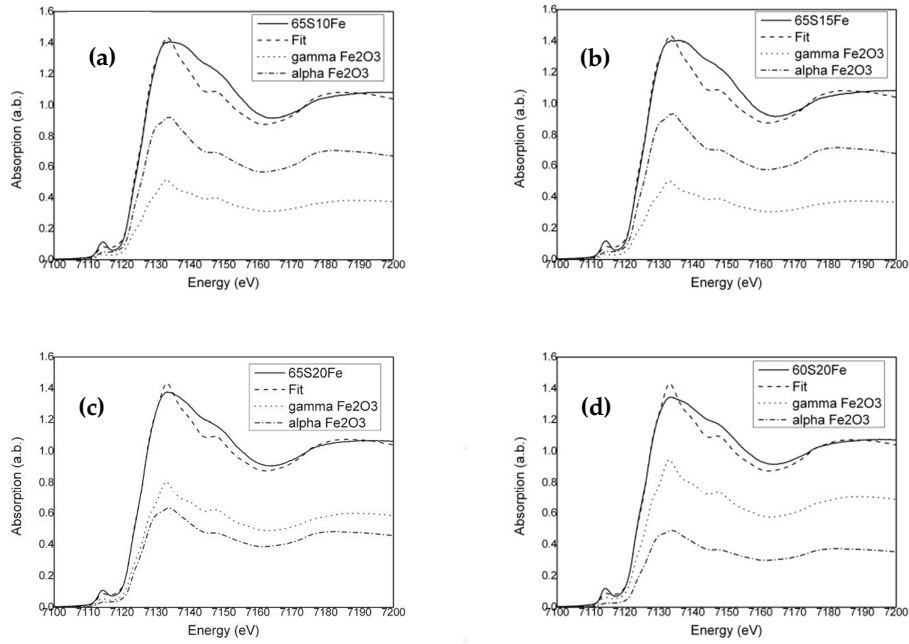
Figure 2. XANES spectra of samples (a) 65S10Fe, (b) 65S15Fe, (c) 65S20Fe and (d) 60S20Fe compared with LCF fits by α-Fe_2O_3 and γ-Fe_2O_3 standards

addition of the magnetic phase may be detrimental to bioactivity in bioactive glasses, this finding demonstrates that the bioactivity can be improved by promoting the γ-Fe_2O_3 phase [11].
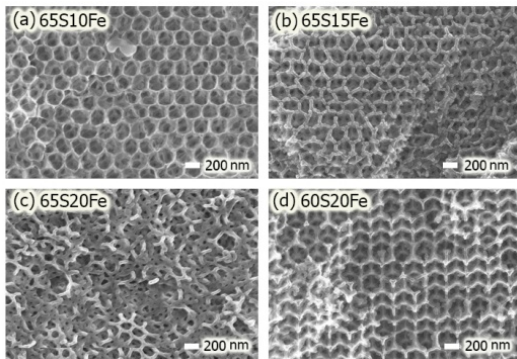

Figure 3. FESEM images showing porous networks in samples (a) 65S10Fe, (b) 65S15Fe, (c) 65S20Fe and (d) 60S20Fe
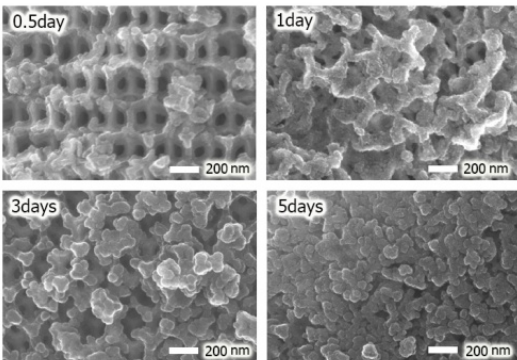

Figure 4. FESEM images showing the successive growth of the apatite phase on samples 65S15Fe after soaking in SBF solution for 0.5, 1, 3 and 5 days
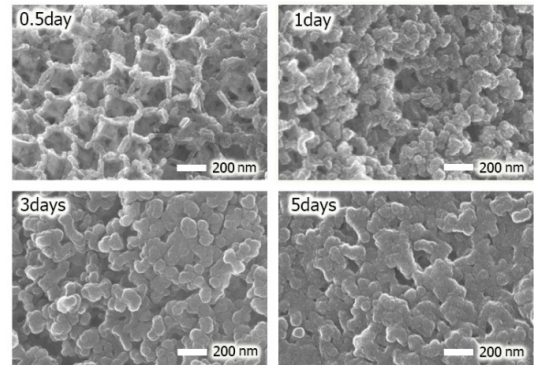

Figure 5. FESEM images showing the successive growth of the apatite phase on samples 60S20Fe after soaking in SBF solution for 0.5, 1, 3 and 5 days
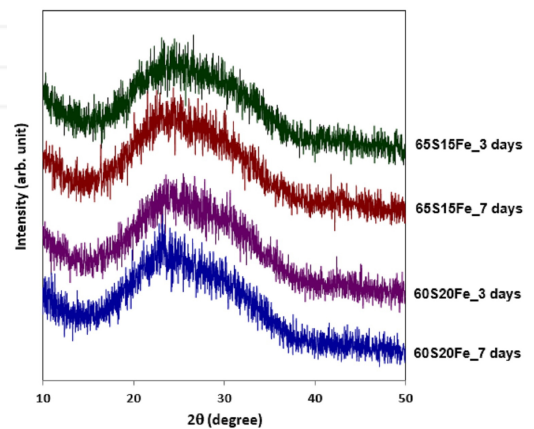

Figure 6. XRD patterns showing the structural phase in samples 65S15Fe and 60S20Fe after soaking in SBF solution for 3 and 7 days

After soaking in SBF solution for three and seven days, neither sample 65S15Fe nor 60S20Fe exhibits sharp charac-
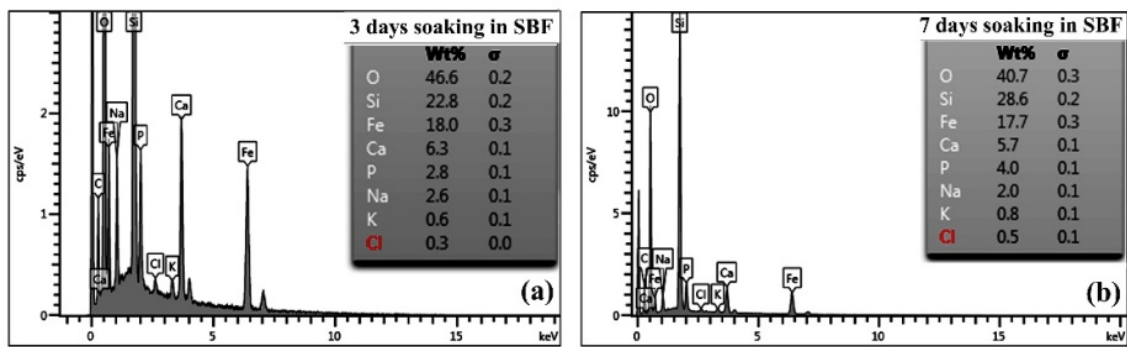
Figure 7. EDS spectra comparing elemental compositions in sample 60S20Fe after soaking in SBF solution for (a) 3 and (b) 7 days

teristic XRD peaks (Figure 6). The appearance of patterns is related to the amorphous silicate phases [8, 13]. Whereas the crystalline phases are not identified by XRD, the EDS spectra indicate the composition of Fe among the common bioactive glass elements, i.e., Si, Ca, Na, P, and O. As compared with Figure 7, the reaction of apatite forming between three and seven days of soaking in SBF solutions changes the compositions. The decreases in Ca and Na are due to the reaction of ion exchanges, with the substantial increase in P signifying the formation of bone-like apatite [3]. Nevertheless, Fe remains fairly constant, at around 18%wt. in sample 60S20Fe.

4. Conclusions

Magnetic macro/mesoporous bioactive glasses with a potential application in bone cancer treatments were derived by one-pot sol-gel synthesis. The increase in $Fe(NO_3)_3$ $9H_2O$ as the starting reagent from 10 to 20% mol enhanced the magnetization of the bioactive glass scaffolds. According to synchrotron XANES analysis, the superparamagnetic properties were due to the mixed iron oxide phase. Different contributions of α-Fe_2O_3 and γ-Fe_2O_3 also led to different rates in the formation of bone-like apatite in the SBF. Such bioactivity was apparent in the changes in surface images and elemental compositions. The variation in bioactivity and magnetic properties of these porous bioactive glass scaffolds were explained in terms of the differences between α-Fe_2O_3 and γ-Fe_2O_3 properties.

5. Acknowledgements

6. References

[1] Gao C, Deng Y, Feng P, Mao Z, Li P, Yang B, Deng J, Cao Y, Shuai C, Peng S (2014) Current progress in bioactive ceramic scaffolds for bone repair and regeneration. Int. J. Mol. Sci. 15:4714–4732.

[2] Gerhardt J L C, Boccaccini A R (2010) Bioactive glass and glass-ceramic scaffolds for bone tissue engineering. Materials. 3:3867–910.

[3] Wu C, Chang J (2012) Mesoporous bioactive glasses: Structure characteristics, drug/growth factor delivery and bone regeneration application. Interface Focus. 2:292–306.

[4] Izadi S, Hesaraki S, Hafezi-Ardakani M (2015) Production of bioactive glass-derived scaffolds using citric acid porogen. Int. J. Mater. Res. 106:301–306.

[5] Kamalian R, Yazdanpanah A, Moztarzadeh F, Ravarian R, Moztarzadeh Z, Tahmasbi M, Mozafari M (2012) Synthesis and characterization of bioactive glass/forsterite nanocomposites for bone and dental implants. Ceram.-Silikaty. 56:331–340.

[6] Hashmi MU, Shah SA, Umer F, Alkedy AS (2013) Effect of sintering temperature on microstructure and *in vitro* behavior of bioactive glass-ceramics. Ceram.-Silikaty. 57:313–318.

[7] Shankhwar N, Singh R K, Kothiyal G P, Perumal A, Srinivasan A (2014) Evolution of magnetic properties of CaO-P_2O_5–Na_2O-Fe_2O_3–SiO_2 glass upon heat treatment. IEEE Trans. Magn. 50:4003504.

[8] Wang D, Lin H, Jiang J, Han X, Guo W, Wu X, Jin Y, Qu F (2013) One-pot synthesis of magnetic, macro/mesoporous bioactive glasses for bone tissue engineering. Sci. Technol. Adv. Mater. 14:025004.

[9] Wu C, Fan W, Zhu Y, Gelinsky M, Chang J, Cuniberti G, Albrecht V, Friis T, Xiao Y (2011) Multifunctional magnetic mesoporous bioactive glass scaffolds with a hierarchical pore structure. Acta Biomater. 7:3563–3572.

[10] Jayalekshmi A C, Victor S P, Sharma C P (2013) Magnetic and degradable polymer/bioactive glass composite nanoparticles for biomedical applications. Colloids Surf. B: Biointerfaces. 101:196–204.

[11] Li X, Wang X, Hua Z, Shi J (2008) One-pot synthesis of magnetic and mesoporous bioactive glass composites and their sustained drug release property. Acta Mater. 56:3260–3265.

Thanida Charoensuk, Wanwisa Limphirat, Chitnarong Sirisathitkul, Witoon Tangwatanakul, Pongsakorn Jantaratana and Upsorn Boonyang: Synchrotron X-ray Absorption and *In Vitro* Bioactivity of Magnetic Macro/Mesoporous Bioactive Glasses

5

[12] Li G, Feng S, Zhou D (2011) Magnetic bioactive glass ceramic in the system CaO-P$_2$O$_5$-SiO$_2$-MgO-CaF$_2$-MnO$_2$-Fe$_2$O$_3$ for hyperthermia treatment of bone tumor. J. Mater. Sci.: Mater. Med. 22:2197–2206.

[13] Zhu M, Zhang J, Zhou Y, Liu Y, He X, Tao C, Zhu Y (2013) Preparation and characterization of magnetic mesoporous bioactive glass/carbon composite scaffolds. J. Chem. 2013: 893479.

[14] Baikousi M, Agathopoulos S, Panagiotopoulos I, Georgoulis A D, Louloudi M, Karakassides M A (2008) Synthesis and characterization of sol–gel derived bioactive CaO–SiO$_2$–P$_2$O$_5$ glasses containing magnetic nanoparticles. J. Sol-Gel Sci. Technol. 47:95–101.

[15] Singh R K, Kothiyal G P, Srinivasan A (2009) *In vitro* evaluation of bioactivity of CaO–SiO$_2$–P$_2$O$_5$–Na$_2$O–Fe$_2$O$_3$ glasses. Appl. Surf. Sci. 255:6827–6831.

[16] Singh R K, Srinivasan A (2011) Magnetic properties of bioactive glass-ceramics containing nanocrystalline zinc ferrite. J. Magn. Magn. Mater. 323:330–333.

[17] Leventouri T, Kis A C, Thompson J R, Anderson I M (2005) Structure, microstructure, and magnetism in ferrimagnetic bioceramics. Biomaterials. 26:4924–4931.

[18] Ravel B, Newville M (2005) Athena, Artemis, Hephaestus: data analysis for X-ray absorption spectroscopy using IFEFFIT. J. Synchrotron Rad. 12:537–541.

[19] Kokubo T, Takadama H (2006) How useful is SBF in predicting in vivo bone bioactivity? Biomaterials. 27:2907–2915.

[20] Charoensuk T, Boonyang U, Sirisathitkul C, Panchawirat P, Senthongkaew P (2014) Effect of sol-gel ageing time on three dimensionally ordered macroporous structure of 80SiO$_2$-15CaO-5P$_2$O$_5$ bioactive glasses. Mater. Sci. Medzg. 20:97–102.

[21] Markides H, Rotherham M, El Haj A J (2012) Biocompatibility and toxicity of magnetic nanoparticles in regenerative medicine. J. Nanomater. 2012:614094.

[22] Singh N, Jenkins G J S, Asadi R, Doak S H (2010) Potential toxicity of superparamagnetic iron oxide nanoparticles (SPION). Nano. Rev. 1:5358.

[23] Layek S, Pandey A, Pandey A, Verma H C (2010) Synthesis of γ–Fe$_2$O$_3$ nanoparticles with crystallographic and magnetic texture. Int. J. Eng. Sci. Technol. 2:33–39.

[24] Cheng W, Tang K, Qi Y, Sheng J, Liu Z (2010) One-step synthesis of superparamagnetic monodisperse porous Fe$_3$O$_4$ hollow and core-shell spheres. J. Mater. Chem. 20:1799–1805.